Drying Regime Maps for Particulate Coatings

Christine M. Cardinal
Dept. of Chemical Engineering and Materials Science, University of Minnesota, Minneapolis, MN 55455

Yoon Dong Jung and Kyung Hyun Ahn
Dept. of Chemical and Biological Engineering, Seoul National University, Seoul, Korea

L. F. Francis
Dept. of Chemical Engineering and Materials Science, University of Minnesota, Minneapolis, MN 55455

DOI 10.1002/aic.12190
Published online February 24, 2010 in Wiley Online Library (wileyonlinelibrary.com).

Key microstructural properties of particulate coatings such as porosity and particle order are established during drying. Therefore, understanding the evolution of particulate distributions during drying is useful for designing coating properties. Here, a 1D model is proposed for the particle distribution through the coating thickness at different drying times and conditions, including Brownian diffusion, sedimentation, and evaporation. Effects of particle concentration on diffusion and sedimentation rates are included. Results are condensed onto a drying regime map which predicts the presence of particle surface accumulation or sediment based on two dimensionless numbers: the Peclet number and the sedimentation number. Cryogenic scanning electron microscopy (cryoSEM) is used to image the transient particulate distributions during the drying of a model system comprised of monodisperse silica particles in water. Particle size and evaporation rates are altered to access various domains of the drying map. There is good agreement between cryoSEM observations and model predictions. © 2010 American Institute of Chemical Engineers *AIChE J,* 56: 2769–2780, 2010
Keywords: colloids, drying, setting/sedimentation, cryoSEM, coatings

Introduction

Particulate coatings are ubiquitous. Often unnoticed by the consumer, they make everyday objects scratch resistant, less reflective, colorful, or hydrophobic. Although the chemistry of these coatings is important, oftentimes their microstructure is just as influential in determining overall functionality. For example, the arrangement of carbon particles in a fuel cell electrode determines the permeability of the coating to reactive hydrogen and oxygen as well as the conductivity of the electrode.[1] Ordered colloidal crystal coatings are created either by slow sedimentation of monodisperse particles[2,3] or by evaporative assembly.[4] A porous particulate coating applied to paper aids in ink adsorption.[5] The required microstructure that makes these coatings functional develops as the dispersion of particulates suspended in a liquid dries into a solid film. Essential qualities, such as porosity, strength, gloss, adhesiveness, particulate order, and concentration gradients, can all be tailored if the connections between the particle distribution and the drying is understood.

As a particulate coating dries, evaporation, diffusion, and sedimentation influence the particle distribution. Evaporation causes the coating free surface to move toward the substrate with velocity E, increasing the particle concentration in the coating over time. (See Figure 1). Particles can accumulate at the descending free surface in what is often termed a "consolidation front".[6] Thermal Brownian diffusion of particles with velocity V_D acts to eliminate concentration gradients that develop. Finally, if the particles are more dense than the surrounding medium, they can sediment with velocity U. The

Christine M. Cardinal and Yoon Dong Jung contributed equally to this work.
Correspondence concerning this article should be addressed to L. F. Francis at lfrancis@umn.edu.

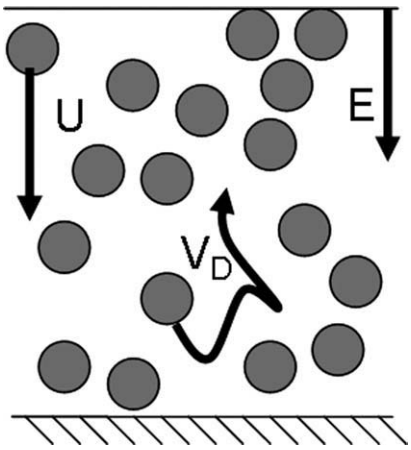

Figure 1. Schematic diagram showing sedimentation (*U*), evaporation (*E*) and diffusion (V_D) in a drying particulate coating.

balance between these three motions determines whether concentration gradients develop through the coating as it dries. Concentration gradients in a drying coating often lead to property variations through the thickness of the final product and can also influence particle arrangement and packing. Concentration gradients can be undesirable, but they can also be beneficial, such as in the design of layered microstructures in coatings containing more than one type of particle.

The balance between E, V_D, and U is most usefully described through dimensionless numbers. The dimensionless Peclet number is used to describe the importance of evaporation to diffusion in a film of initial thickness H_0.[7] It is given as

$$Pe = \frac{EH_0}{D_0} \tag{1}$$

where D_0 is the Stokes-Einstein diffusion coefficient, defined as:

$$D_0 = \frac{kT}{6\pi\mu R} \tag{2}$$

for a spherical particle of radius R dispersed in a liquid with viscosity μ and temperature T. The Botzmann constant is k. Routh and Zimmerman[8] examined the effects of evaporation with respect to diffusion using a 1D model. When evaporation is dominant ($Pe \gg 1$), the model predicts that consolidation fronts form at the air–water interface and grow in thickness as the free surface descends toward the substrate until the entire coating reaches the maximum packing fraction. When diffusion dominates ($Pe \ll 1$), the particle concentration is predicted to remain approximately uniform through the coating thickness as it dries. Similar models have been adapted to include particle charge[9] and Marangoni flows, which are common in solvent borne coatings.[10]

Limited experimental methods exist to assess the concentration gradients that develop during the active drying of coatings. The effects of varying Pe on particle distributions in coatings have been studied experimentally using magnetic resonance (MR) profiling, which can be used to track concentrations of water in a drying film to a resolution of about 10 μm.[11,12] This technique confirmed predictions that water concentration gradients occur in a drying film when $Pe > 1$. Specifically, MR profiling confirmed theoretical predictions that the water concentration gradient between the consolidation front and the bulk of the film scales with $Pe^{1/2}$.[13] Raman spectroscopy is another experimental technique able to obtain concentration profiles in real time, as long as the coating is relatively clear and the species are Raman active.[14] Cryogenic scanning electron microscopy (cryoSEM) has also been successfully used to image consolidation front growth in particulate coatings.[6] By vitrifying the coating in liquid ethane before it is completely dry, the microstructure of the coating can be frozen in time and imaged in a scanning electron microscope on a temperature-controlled stage. By imaging specimens frozen after different extents of drying, the developing microstructure can be characterized. In this way, Luo et al.[15] studied the effects of varying drying rate on the microstructure formation of a large latex/small silica blend. As these MR and cryoSEM studies were primarily focused on predicting the particle distribution of latex coatings, the effects of sedimentation were ignored.

The first model describing the sedimentation of particles was formulated by Kynch,[16] who showed that there are three main regions in a sedimenting suspension: the sediment near the bottom, a region where the concentration equals the initial concentration, and a particle free-zone at the top. This model has been adapted for colloidal systems that experience diffusion.[17,18] The strength of sedimentation is compared to diffusion using the sedimentation Peclet number,

$$Pe_{\text{sed}} = \frac{U_0 H_0}{D_0} \tag{3}$$

where U_0 is the Stokes settling velocity of a spherical particle of density ρ_P in a dilute solution of liquid with density ρ_L and viscosity μ_L, under gravitational acceleration g:

$$U_0 = \frac{2R^2 g(\rho_p - \rho_L)}{9\mu_L} \tag{4}$$

Increasing the strength of diffusion (decreasing Pe_{sed}) softens the boundaries between the three concentration regions. Various researchers have experimentally observed the effects of varying Pe_{sed} on the sedimentation of colloidal suspensions over centimeter sized distances in the absence of evaporation using techniques such as light extinction[19] X-ray tomography,[20] and light scattering.[21] Experiments agreed well with models.

Although the effects of varying Pe and Pe_{sed} have been studied independently, sedimentation, diffusion, and evaporation have not yet been studied together for coating systems. Because many researchers do not have the means to observe coating microstructure during drying, the path of the microstructure development is often indirectly inferred from final coating appearance rather than designed intelligently. Therefore, the goal of this article is to create a drying map that predicts the drying regime (sedimentation, diffusion, or evaporation dominant) based on Pe and the sedimentation number, N_s, which describes the strength of sedimentation to evaporation:

$$N_s = \frac{U_0}{E} = \frac{Pe_{\text{sed}}}{Pe}. \tag{5}$$

As these two dimensionless quantities are defined using infinite dilution quantities U_0 and D_0, these parameters do not

change with time or concentration for a given coating. Consequently, calculating Pe, Pe_{sed}, and N_s is simple for any coating and drying process and yet can give great insights into how a coating microstructure will develop. Although the drying map is created by solving the full 1D conservation equation, it is shown that the boundaries between drying regimes can be approximated through simple functions of the initial particle volume fraction. This map is then explored experimentally to demonstrate how drying conditions and particle properties affect the microstructure development of a model particulate coating system. Using cryoSEM, the particulates within the coating are imaged at various time points during the drying process. Finally, the drying map is used to demonstrate how novel coatings can be engineered.

Theory

The particle volume fraction as a function of position and time within a drying coating containing a volatile liquid and particles is obtained by solving the particle conservation equation, adapted from Russel et al.[22] When the coating thickness is small relative to its lateral dimensions, the drying of a particulate coating is assumed to be a one dimensional process. The 1D conservation equation describing the particle volume concentration (ϕ) in a particulate coating during the drying process, including diffusion, evaporation, and sedimentation, is expressed as:

$$\frac{\partial \phi}{\partial t} = \frac{\partial}{\partial y}\left(U\phi + D\frac{\partial \phi}{\partial y}\right). \tag{6}$$

A no-flux boundary condition is applied at the substrate ($y = 0$). At the top surface ($y = H_0 - Et$) there is an effective particle flux into the coating due to evaporation:

$$y = 0, \quad U\phi + D\frac{\partial \phi}{\partial y} = 0 \tag{7}$$

$$y = H_0 - Et, \quad U\phi + D\frac{\partial \phi}{\partial y} = E\phi \tag{8}$$

where H_0 is the initial coating thickness, E is the evaporation rate given in terms of free surface velocity, D is the particle mutual diffusion coefficient, and U is the particulate sedimentation velocity.

The effects of particle concentration on D and U are described through the sedimentation coefficient, K(ϕ), which describes hydrodynamic interactions, and the compressibility factor, Z(ϕ), which represents the concentration dependence of the osmotic pressure gradient for hard sphere particles. Both parameters are strong functions of ϕ.

$$D(\phi) = K(\phi)\frac{d}{d\phi}[\phi Z(\phi)]D_0, \quad D_0 = \frac{kT}{6\pi\mu R} \tag{9}$$

$$U(\phi) = K(\phi)U_0, \quad U_0 = \frac{2R^2 g(\rho_p - \rho_L)}{9\mu} \tag{10}$$

The sedimentation coefficient $K(\phi)$ has a functional form $K(\phi) = (1-\phi)^{6.55}$.[22] This equation was shown experimentally to satisfactorily represent the dependence of sedimentation speed on concentration for the model system. The compressibility factor, $Z(\phi)$, takes the general form[8,22] $Z(\phi) = \frac{1}{(\phi_m - \phi)}$ where ϕ_m is the maximum value of ϕ. This form of compressibility factor captures the divergence of the diffusion coefficient near the particle maximum packing fraction due to increased particle collisions and maintains appropriate values near the dilute limit. The maximum packing fraction was chosen to be $\phi_m = 0.64$, assuming random close packing of the particles. Both the sedimentation coefficient and the compressibility factor assume that the particles interact as hard spheres.

The conservation equation is nondimensionalized with

$$\bar{t} = \frac{t}{H_0/E} \quad \text{and} \quad \bar{y} = \frac{y}{H_0}. \tag{11}$$

$$\frac{\partial \phi}{\partial \bar{t}} = \frac{\partial}{\partial \bar{y}}\left[N_s K(\phi)\phi + \frac{1}{Pe}K(\phi)\frac{d}{d\phi}[\phi Z(\phi)]\frac{\partial \phi}{\partial \bar{y}}\right] \tag{12}$$

$$\bar{y} = 0, \quad N_s K(\phi)\phi + \frac{1}{Pe}K(\phi)\frac{d}{d\phi}[\phi Z(\phi)]\frac{\partial \phi}{\partial \bar{y}} = 0 \tag{13}$$

$$\bar{y} = 1 - \bar{t}, \quad N_s K(\phi)\phi + \frac{1}{Pe}K(\phi)\frac{d}{d\phi}[\phi Z(\phi)]\frac{\partial \phi}{\partial \bar{y}} = \phi \tag{14}$$

Nondimensionalization reveals the two main dimensionless variables discussed in this report, Pe and N_s. These equations are valid up to the time when the entire coating is packed with maximum packing ϕ_m. This dimensionless time, $\bar{t}_m$, is given by:

$$\bar{t}_m = \frac{\phi_m - \phi_0}{\phi_m}. \tag{15}$$

A shrinking coordinate system with a dimensionless shrinking velocity of 1 was used to fix the free surface boundary. The shrinking space and time coordinates are defined by:

$$\xi = \frac{\bar{y}}{1 - \bar{t}}, \quad \tau = \bar{t}. \tag{16}$$

The dimensionless conservation equation and boundary conditions in the shrinking coordinate system are:

$$\frac{\partial \phi}{\partial \tau} + \frac{\xi}{1-\tau}\frac{\partial \phi}{\partial \xi} = \frac{N_s}{(1-\tau)}\frac{\partial}{\partial \xi}[K(\phi)\phi] + \frac{1}{Pe(1-\tau)^2}\frac{\partial}{\partial \xi}\left[K(\phi)\frac{d}{d\phi}[\phi Z(\phi)]\frac{\partial \phi}{\partial \xi}\right] \tag{17}$$

$$\xi = 0, \quad N_s Pe\phi(1-\tau) + \frac{d}{d\phi}[\phi Z(\phi)]\frac{\partial \phi}{\partial \xi} = 0 \tag{18}$$

$$\xi = 1, \quad N_s PeK(\phi)\phi(1-\tau) + K(\phi)\frac{d}{d\phi}[\phi Z(\phi)]\frac{\partial \phi}{\partial \xi} = Pe(1-\tau)\phi. \tag{19}$$

Equations 17–19 describe the particle distribution before the liquid recedes into the packed particles. After the liquid enters the packing, capillary effects must be taken into account. These effects and their implications on the structure of packings of deformable particles have been modeled by

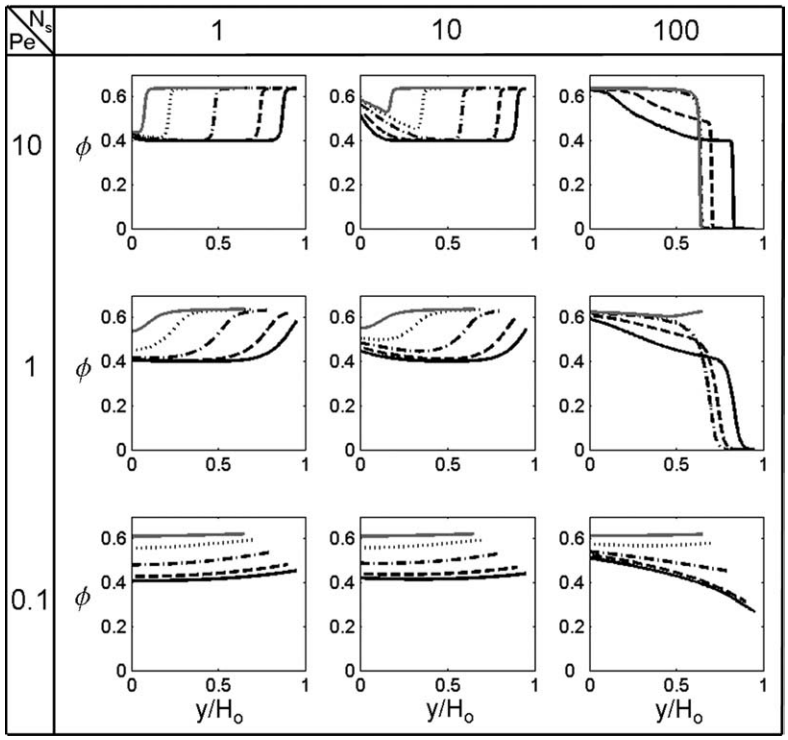

Figure 2. Particle volume fraction (ϕ) profiles for various N_s and Pe with respect to the fixed coordinate y/H_0 at various dimensionless times: $\bar{t} = 0.05$ (—), $\bar{t} = 0.1$ (---), $\bar{t} = 0.2$ (-.-.), and $\bar{t} = 0.3$ (....), $\bar{t} = 0.35$ (—).

Initial volume fraction: $\phi_0 = 0.4$.

Routh and Russel.[23] Specifically, they have created a process map that identifies conditions when a packed particle layer at the free surface deforms into a dense skin.

Numerical Method

The dimensionless conservation equation in shrinking coordinates was solved numerically using COMSOL Multiphysics 3.2. The PDE General Form Application Mode with Direct (UMFPACK) Linear system solver was used. The model has 480 elements and a 10^{-5} time step size that gave sufficient accuracy for most cases. Other settings were the default values of COMSOL. Two limiting cases of the conservation equation were verified with known numerical solutions: the distribution of particles during solvent evaporation from coatings,[8] and an asymptotic description of transient settling and ultrafiltration of colloidal dispersions.[18]

Experimental Procedures

A model system of monodisperse silica particles in water was used for an experimental comparison to the theoretical model. Monodisperse silica particles with diameters ranging from 200 nm to 1 μm were synthesized using the Stober method.[24,25] Particles were washed after synthesis and suspended in distilled water at pH 10 with various initial volume fractions. The density of the particles was measured through water displacement to be 1.9 g/cm^3. Additionally, monodisperse silica particles of 1 μm $\pm$ 1.5% diameter (Monosphere, Merck) and density of 2.2 g/cm^3 were also used.

Controlled volumes of coating suspension were spread on 5 $\times$ 7-mm silicon substrates using a micropipette, and samples were allowed to dry for various times in still air or under forced air. By controlling the drying environment, the evaporation rate, E, could be varied from 1.5 to 100 μm/min. Drying rates were determined by measuring the coating thickness over time from cryoSEM images.

The particle distribution within the coatings was imaged using cryoSEM. After samples had dried for various amounts of time, the coatings were plunged into liquid ethane at -196°C for vitrification. Samples were then transferred to an Emitech K-1250 cryo preparation chamber where they were fractured at -120°C under liquid nitrogen to expose the coating cross-section, sublimed at -96°C for 5–7 min to reveal the particles, and sputter coated with a 2 nm layer of platinum to reduce charging in the electron microscope. Finally, samples were imaged in a Hitachi S4700 FESEM at -160°C. In most cases, samples dried edge-in and top-down; therefore, all data and images were taken as close to the middle of the coating as possible.

Results and Discussion

Numerical results

Figure 2 shows particle concentration profiles calculated based on Eq. 17 for Pe ranging from 0.1 to 10 and N_s ranging from 1 to 100 with $\phi_0 = 0.4$. As the coating dries, the coating thickness reduces and the particle volume fraction approaches the maximum packing fraction, $\phi_m = 0.64$, at long drying times. At intermediate times, the concentration

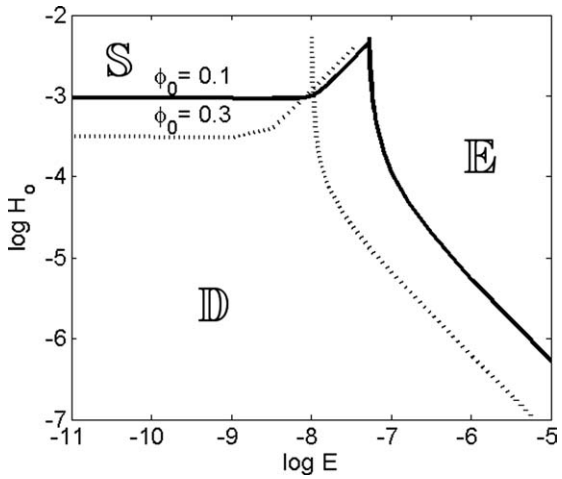

Figure 3. Drying regime map based on dimensional coordinates: initial coating thickness H_0 (m) and evaporation rate E (m/s).

The effect of initial particle volume fraction is shown for an aqueous coating containing silica particles ($R = 200$ nm) ($\mathbb{S}$ = sedimentation, $\mathbb{E}$ = evaporation, $\mathbb{D}$ = diffusion).

profile within the coating is significantly affected by the relative magnitudes of N_s and Pe. Two main cases are discussed here: low N_s, where the tendency for sedimentation is small relative to evaporation and high N_s where sedimentation overwhelms evaporation.

At low N_s, ($N_s = 1$) where sedimentation is weak, the concentration profile through the depth of the coating reflects the competition between evaporation and diffusion. This competition is described by Pe. Increasing Pe, which corresponds to increasing evaporation rate, coating thickness, or particle radius, increases the importance of evaporation on particle distribution. In an evaporation dominant coating, the suspension-air free surface descends quickly toward the substrate faster than particles can diffuse away. Consequently, particles accumulate at the free surface in a drying front. As evaporation proceeds, the coating thickness shrinks, and the thickness of the front grows toward the substrate until the entire coating is at the maximum packing fraction. These results concur with previous researchers.[7] Conversely, at low N_s and low Pe, diffusion dominates over evaporation, and the particle concentration remains homogeneous through the depth of the coating as it dries.

At high N_s, ($N_s = 100$) where evaporation is slow, the concentration profile is determined by a competition between sedimentation and diffusion. At high Pe, where sedimentation is strongest, particles fall toward the substrate faster than the free-surface descends, creating a particle-free zone near the air–suspension interface. Particles accumulate at the substrate, and the resulting concentration slows their speed of descent according to Eq. 10. Also, the strength of diffusion is increased dramatically at concentrations approaching the maximum packing fraction, reflecting the sediment compressibility.[17,18] These two factors create a transition region of gradually increasing concentration between the initial-concentration zone and the sediment. This phenomenon is stronger at lower Pe, where the diffusion coefficient and its dependence on concentration are significant. At very low Pe, just as in the low N_s case, diffusion is strong and the particle concentration is uniform through the coating thickness throughout the drying. These results also agree with previous work.[18]

At intermediate N_s values, sedimentation and evaporation behaviors are both important in the drying of the coating. Particles concentrate at the top and the bottom of the coating, whereas the center remains near the initial volume fraction of particles. Increasing the strength of sedimentation (increasing N_s) at a constant Pe decreases the rate of particle accumulation at the top surface by creating a downward flux of particles.

Drying Regime Maps—logH_0 vs. logE

To understand the effects of changing, the process conditions on the drying behavior, drying maps were created to predict evaporation, sedimentation, or diffusion dominance for a given initial coating thickness and evaporation rate. These maps were inspired by the work of Cairncross et al[26] on the drying regime maps for sol–gel coatings. In Figures 3 and 4, the black lines represent the conditions where the local particle concentration at the top or the bottom of the coating reaches 90% of the maximum packing fraction in less than half the time required for the entire coating to reach that concentration.

$$\phi\left(\xi = 0, t = \frac{\bar{t}_m}{2}\right) \geq 0.9\phi_m \quad \text{Sediment} \tag{20a}$$

$$\phi\left(\xi = 1, t = \frac{\bar{t}_m}{2}\right) \geq 0.9\phi_m \quad \text{Skin} \tag{20b}$$

When this accumulation occurs at the top of the coating, evaporation dominates and the region of the map that

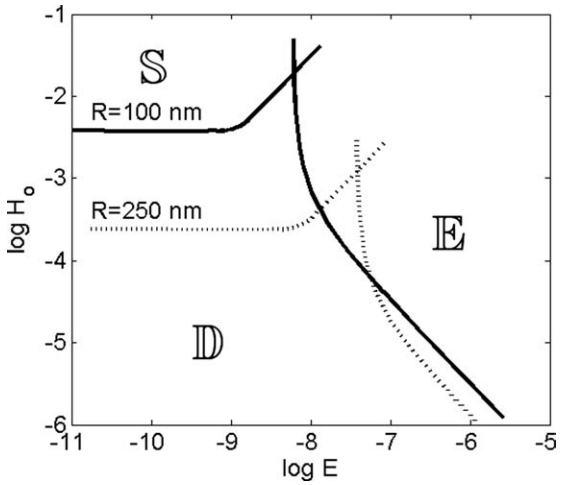

Figure 4. Drying regime map based on dimensional coordinates: initial coating thickness H_0 (m) and evaporation rate E (m/s).

The effect of silica particle size is shown for an aqueous dispersion with $\phi_0 = 0.2$ ($\mathbb{S}$ = sedimentation, $\mathbb{E}$ = evaporation, $\mathbb{D}$ = diffusion).

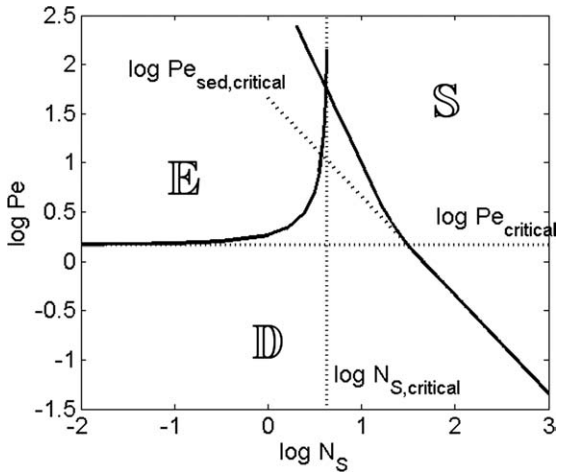

Figure 5. Drying regime map based on dimensionless coordinates Peclet number (*Pe*) and sedimentation number (N_s).

Evaporation (𝔼), sedimentation (𝕊), and diffusion (𝔻) dominant regions are shown for a coating with ($\phi_0 = 0.2$). Critical values are also marked for limiting cases.

borders this condition is called the "evaporation regime" and is labeled "𝔼" In this article, top surface particle accumulation is termed a "skin," although the influence of particle accumulation on the evaporation rate is not modeled. Not surprisingly, evaporation tends to dominate for coatings dried at higher rates. Particle accumulation at the base forms a "sediment," which defines the "sedimentation" drying regime ("𝕊"). Sedimentation is found at increased coating thickness, where particles have more time to sediment before the overall particle concentration reaches the maximum packing fraction. At relatively low evaporation rates, the diffusion of particles is the dominant motion in the coating; this region is the diffusion drying regime ("𝔻"). At limited conditions, the evaporation and sedimentation regions overlap, indicating that accumulation occur at both the top and the bottom of the coating as it dries.

Figure 3 shows the effect of initial volume fraction in the coating dispersion. As the initial volume fraction decreases, hydrodynamic and particle interactions decrease and speed the sedimentation and diffusion rates. Using the current model, diffusion rates are approximately twice as fast at $\phi = 0.1$ than at $\phi = 0.3$, meaning that higher evaporation rates are necessary to promote skin formation in less concentrated coatings. Also, decreased particle concentration corresponds to a decreased number of particles that are accumulated at the coating surface for a given amount of evaporation. Similarly, the boundary between sedimentation and diffusion is shifted to increase the size of the diffusion regime at lower particle concentrations, although the overall shape of the boundaries is retained.

Figure 4 compares the drying regimes for coatings containing particles of different sizes. As particle radius increases, the sedimentation rate increases, and sediments form before the entire coating reaches a maximum packing in thinner coatings. As particle radius increases, the strength of diffusion decreases, so at lower evaporation rates skins can form.

Figures 3 and 4 display data comparing individual coating systems and provide an intuitive basis for the drying regimes. However, it would also be useful to have a universal drying map to predict the behavior for a wide variety of coating formulations and conditions.

Drying Regime Maps—log Pe vs. log N_s.

To create a universal map that is applicable to any coating system, evaporation (𝔼), sedimentation (𝕊), and diffusion (𝔻) dominant regimes were found using the same method discussed previously and displayed with respect to the two dimensionless variables: *Pe*, and N_s. An example of a universal map for an initial particle volume fraction of 0.2 is shown in Figure 5. To find a position on the map, one calculates *Pe* and N_s (Eqs. 1 and 5) from measurable parameters: particle radius, R, particle density, ρ_P, liquid density, ρ_L, liquid viscosity, μ, and evaporation rate, E.

As demonstrated with the concentration profiles in Figure 2, the drying behavior can be split into two cases: high and low N_s, with a critical value of N_s ($N_{s,critical}$) that serves as the boundary between these two regimes. At low N_s, where $N_s < N_{s,critical}$, sedimentation is unimportant and evaporation and diffusion compete. Here, there is a critical Peclet number ($Pe_{critical}$) above which an evaporation-induced skin forms. At high N_s, where $N_s > N_{s,critical}$, evaporation is unimportant and sedimentation and diffusion compete. A critical Peclet number is defined for this region ($Pe_{sed,critical}$). $Pe_{sed,critical}$ varies with both N_s and *Pe* and marks the division between the diffusion dominated regime and the sedimentation dominated regime. Interestingly, the line for $Pe_{sed,critical}$ changes slope at $Pe_{critical}$, reflecting the increasing influence of evaporation in that region. A small overlap of the sedimentation and evaporation regions exist where both of these behaviors are predicted to be of consequence.

Figure 6 shows the effect of initial particle concentration on the drying regime map boundaries. Similar to Figures 3 and 4, as the initial volume fraction changes the critical values change, but the shape of drying regime map is retained. As discussed earlier, sedimentation and diffusion regimes are

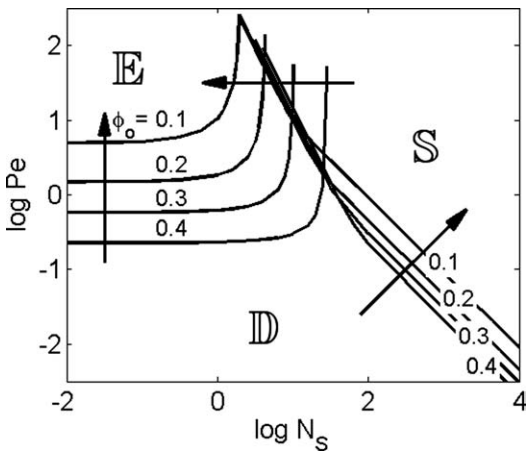

Figure 6. Effect of initial particle volume fraction on the drying regime map based on dimensionless coordinates.

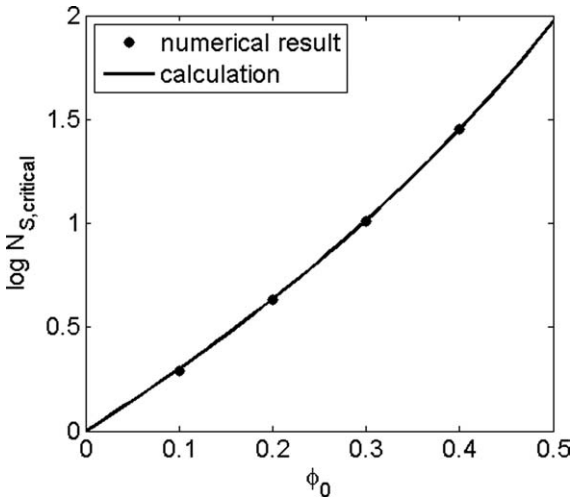

Figure 7. Dependence of $N_{s,critical}$ on initial particle volume fraction found by numerically solving the full conservation equation and an analytical approximation (Eq. 21).

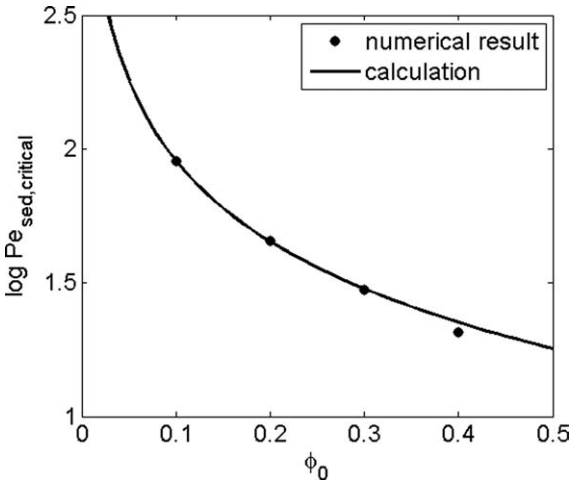

Figure 8. Dependence of $Pe_{sed,critical}$ on the initial particle volume fraction found by numerically solving the full conservation equation and an analytical approximation (Eq. 26).

larger at smaller initial volume fraction. The effects of initial concentration on the boundaries of the drying map can be better understood by analytically solving limiting cases described by the critical dimensionless numbers.

At $N_{s,critical}$, where sedimentation and evaporation are balanced, a skin does not develop because the particle sedimentation rate is exactly equal to the evaporation speed of the air–water interface, or:

$$E \approx U_{top} = U_0 K(\phi_0) \tag{21}$$

$$N_{S,critical} = \frac{U_0}{E} = \frac{U_0}{U_{top}} = \frac{1}{K(\phi_0)}. \tag{22}$$

The predictions of Eq. 22 are compared with numerical results in Figure 7. This equation matches the numerical results well.

In the region of $Pe_{sed,critical}$, diffusion and sedimentation are of equal importance and evaporation does not have much effect. To determine when sedimentation and diffusion are in balance, the steady state conservation equation is solved with boundary conditions changed to reflect the lack of evaporation.

$$0 = \frac{\partial}{\partial \bar{y}}\left[N_s K(\phi)\phi + \frac{1}{Pe}K(\phi)\frac{d}{d\phi}[\phi Z(\phi)]\frac{\partial \phi}{\partial \bar{y}}\right] \tag{23}$$

$$\bar{y} = 0 \text{ or } 1, \quad N_s K(\phi)\phi + \frac{1}{Pe}K(\phi)\frac{d}{d\phi}[\phi Z(\phi)]\frac{\partial \phi}{\partial \bar{y}} = 0 \tag{24}$$

After a single integration of (24), the following is obtained:

$$\int_{\phi(0)}^{\phi(1)} \frac{-1}{PeN_s}\frac{\phi_m}{(\phi_m - \phi)^2}d\phi = \int_1^0 \phi dy \tag{25}$$

Due to mass conservation, the right hand side of Eq. 25 equals ϕ_o.[18] Assuming negligible particle concentration at the top surface of the coating [$\phi(1) = 0$], an expression for the volume fraction at the bottom is obtained.

$$\phi(\bar{y} = 0) = \frac{Pe_{sed}\phi_0\phi_m}{1 + Pe_{sed}\phi_0} \tag{26}$$

$$\text{At } Pe_{sed,critical},\ \phi(\bar{y} = 0) = 0.9\phi_m, \quad \text{so}$$
$$Pe_{sed,critical} = \frac{9}{\phi_0}. \tag{27}$$

Figure 8 shows $Pe_{sed,critical}$ vs. the initial volume fraction found numerically and approximated using Eq. 27. The calculation and the numerical result are almost the same.

In the case of $Pe_{critical}$, a simple calculation does not match the numerical result accurately. No simple analytical solution was obtained; however, Figure 9 shows the important effect of initial volume fraction on $Pe_{critical}$.

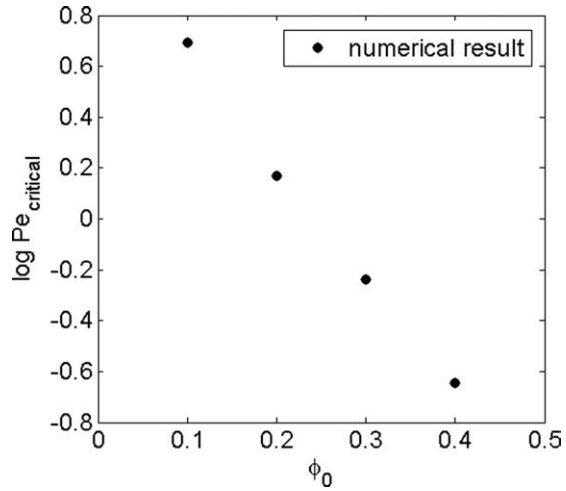

Figure 9. Dependence of $Pe_{critical}$ on initial particle volume fraction found by numerically solving the full conservation equation.

Table 1. Experimentally Explored Coating Conditions

R (nm)	φ_0	E (μm/min)	H_0 (μm)	ρ_p g/cm^3	Observed regime	log(N_s)	log(Pe)
200	0.1	7.8	183	1.9	Evaporation	−0.22	1.4
200	0.2	7.8	183	1.9	Evaporation	−0.22	1.4
91	0.2	2.0	250	1.9	Evaporation	−0.31	0.55
135	0.2	87	600	1.9	Evaporation	−1.6	2.7
200	0.2	62	250	1.9	Evaporation	−1.1	2.4
120	0.1	5.5	200	1.9	Evaporation	−0.51	1.0
50	0.1	5.5	200	2.2	Diffusion	−1.1	0.63
50	0.1	3.5	223	2.2	Diffusion	−0.95	0.48
500	0.1	22	130	2.2	Sediment/Evap	0.25	2.1
500	0.1	22	211	2.2	Sedimentation	0.25	2.3
500	0.1	2.0	250	2.2	Sedimentation	1.3	1.3
500	0.25	6.6	500	1.9	Sedimentation	0.65	2.1

CryoSEM results

To demonstrate the effectiveness of the drying map to predict the microstructure development of a drying coating, cryoSEM was used to observe the microstructure of a model system under various drying conditions. Several conditions were investigated, as summarized in Table 1. These conditions explore all three regions of the drying map. Accumulation zones were identified and noted if there was a noticeable concentration of particles at either the top or the bottom of the coating when the sample was halfway dry, or as close to this time point as possible. A representative selection of cryoSEM results are presented in Figures 11–14. The drying conditions for these samples are mapped for your convenience on Figure 10.

High evaporation rates and larger initial coating thicknesses tended to produce coatings that dried in the evaporation regime. CryoSEM images (Figure 11) show the evolution of a drying front that is growing in a coating dried in the evaporation regime. A layer of highly concentrated particles at the top of the coating grows with time, as marked by the white bar in the image. The particle concentration below this front stays approximately constant with time, as estimated visually from images. At the top surface of the coating, some particles are ordered. Convective steering[27]

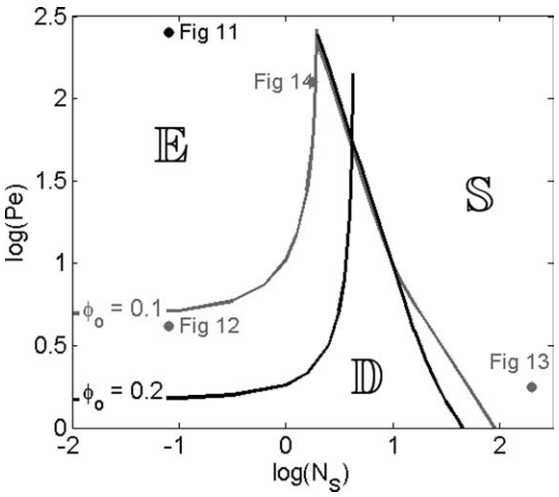

Figure 10. Drying regime map marking *Pe* and N_s corresponding to Figures 11–15.

$\phi_0 = 0.1$ (grey) and $\phi_0 = 0.2$ (black).

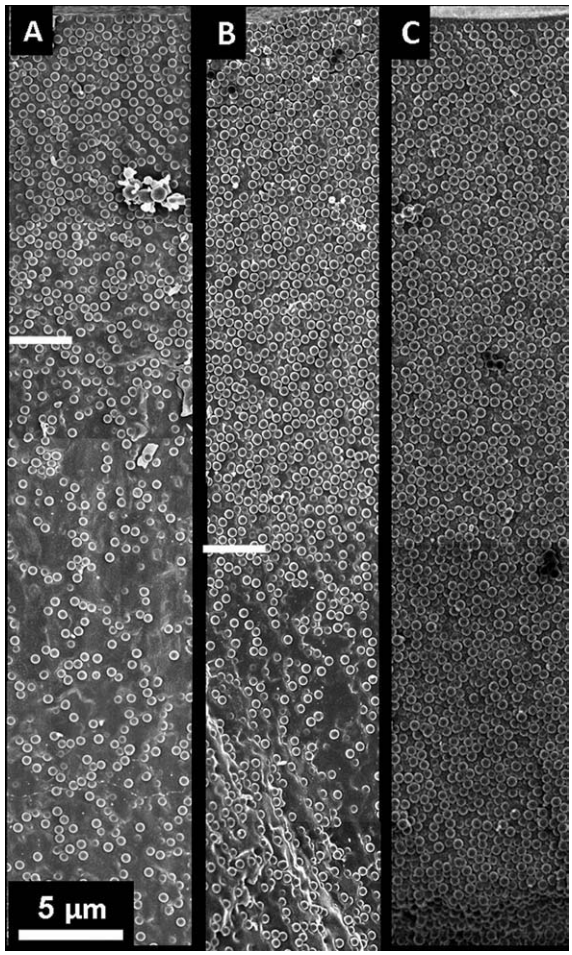

Figure 11. Cross-section cryoSEM images obtained at different time points showing evaporation dominance.

Drying conditions were log(Pe) = 2.4, log(N_s) = −1.1, ϕ_0 = 0.2. Dimensionless drying times and total coating thicknesses were **A**: $\bar{t}$ = 0.3, H = 190 μm; **B**: $\bar{t}$ = 0.4; H = 160 μm **C**: $\bar{t}$ = 0.7 H = 70 μm. A white dash marks the edge of the consolidation front and the suspension-air free surface is at the top of each image.

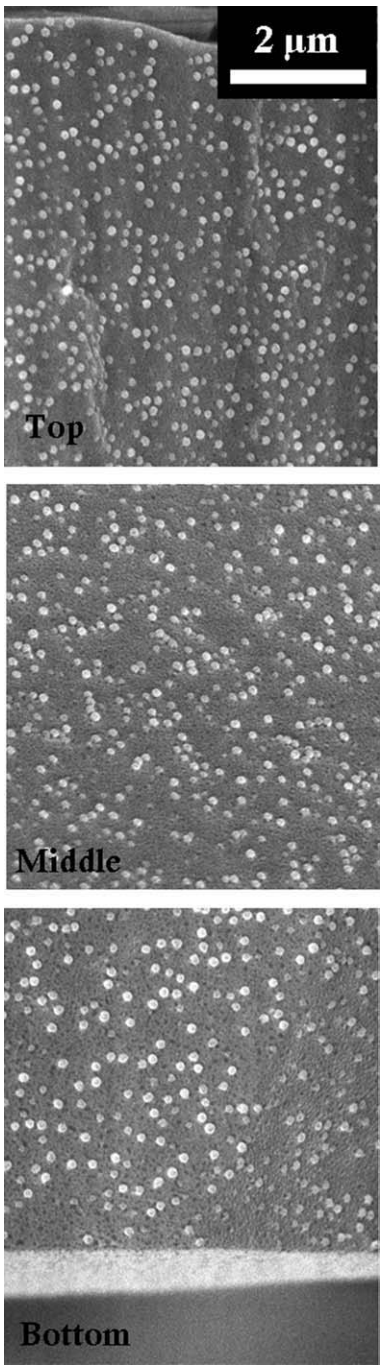

Figure 12. Cross-section cryoSEM image obtained at $\bar{t}$ = 0.4 showing diffusion dominance.

Images were from different depths in the coating, as shown. Drying conditions were $\log(Pe) = 0.62$, $\log(N_s) = -1.1$, $\phi_0 = 0.1$.

and capillary forces at the free surface bring the particles together in an ordered crystal. This effect occurs because the particles are monodisperse. The crystal continues to grow when the time scale for particulate ordering is less than the addition speed of new particulates to the front. At $\bar{t} = 0.7$, the coating is fully consolidated. The top few layers of the final coating are polycrystalline with areas of close packing, whereas the bulk of the film is disordered. Large areas of particulate order may introduce some discrepancy with in the model, which assumes a random maximum packing fraction $\phi_m = 0.64$ instead of the packing fraction most commonly seen for colloidal crystals ($\phi_m = 0.74$). This model would overestimate the necessary Pe to form an ordered skin and overestimate the necessary N_s to form an ordered sediment. As order was most often found only in small amounts through the depth of a skin and never in a sediment, this effect is assumed to be small in analyzing the given system.

If Pe is reduced from the evaporation regime by decreasing the drying rate or the size of the particles, diffusion plays a larger role in determining the particle distribution. The boundary between the skin and the bulk of the coating was less distinct in coatings that were dried at lower Pe, near the evaporation/diffusion boundary in the drying regime map. Finally, in the diffusion regime, the concentration of particles remains fairly uniform with depth at any point in the drying, as shown in Figure 12.

In the sedimentation regime, large particles settled with a greater velocity than the evaporation velocity of the free surface, creating a region at the top of the coating that was depleted of particles (Figure 13). Below the particle-free

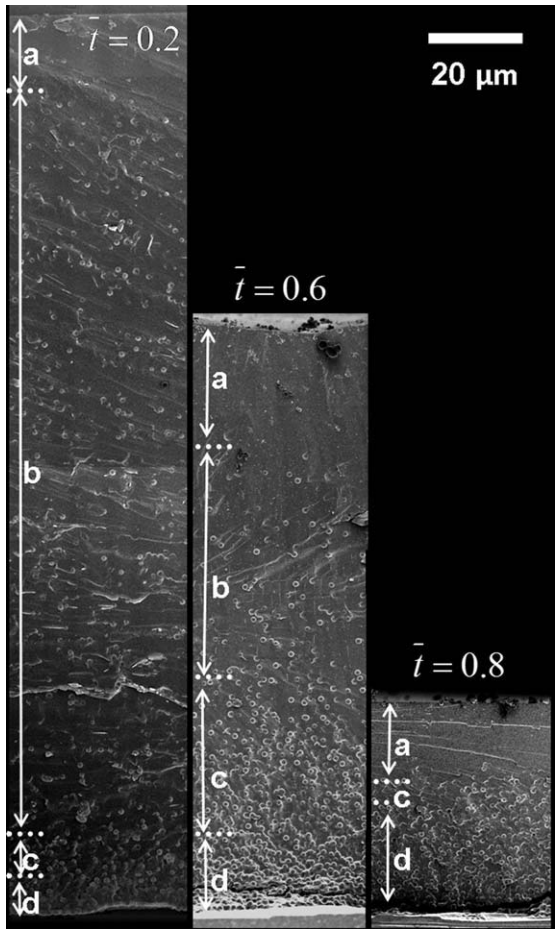

Figure 13. Cross-section cryoSEM images obtained at different times as indicated showing sedimentation.

Drying conditions were $\log(Pe) = 0.25$, $\log(N_s) = 2.3$, $\varphi_0 = 0.1$. Sedimentation zones include (a) a particle-free zone, (b) initial concentration zone (c) a transition zone, and (d) sediment.

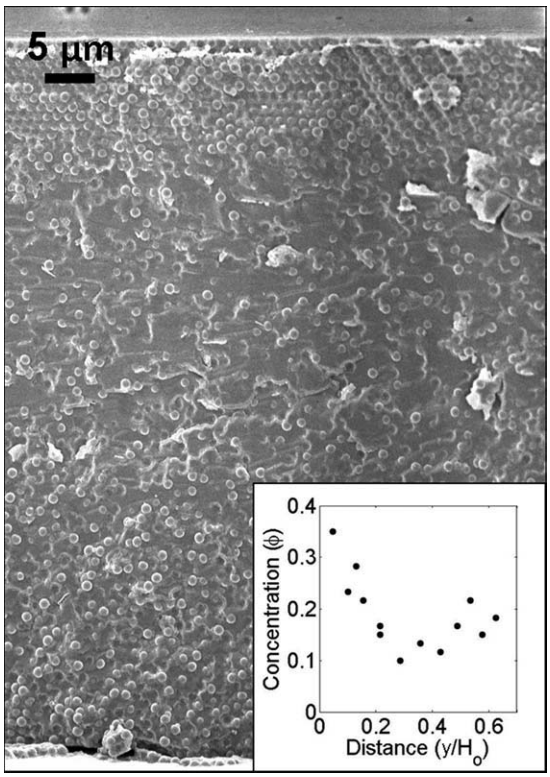

Figure 14. Cross-section cryoSEM image of a coating showing sedimentation and evaporation. $\bar{t}$ = 3.3; Pe = 0.25; N_s = 2.1.

The inset shows the volume fraction of particles as a function of depth in the coating as estimated from the image.

zone was a zone of constant particle concentration, composed of free-falling particles. Near the sediment, the transition zone is clear. As time progresses, the initial concentration zone decreases in length, and the sediment grows until it includes all of the particles. Finally, the air–water interface recedes into the packing.

In the case where the particles in the coating sediment at a speed that is slower than the descent of the free surface, the model predicts that both a sediment and a skin can form simultaneously. This phenomena has been captured in Figure 14. An ordered particle packing appears at the top of the coating. This skin grows until it reaches the sediment near the substrate. Exploiting this phenomenon in more complicated coating systems may lead to inexpensive methods to produce novel coatings.

Conditions where sedimentation, diffusion, and evaporation were observed experimentally are marked on the drying map in Figure 15. The experimental data match the model well, especially the delineation between diffusion and evaporation regimes. The sedimentation regime was found experimentally to occur at slightly lower N_s values than those predicted, corresponding to an underestimation of the sedimentation speed by the model. Lateral drying also influenced the particle distributions, especially at later drying times.[7,28] In this work, care was taken to minimize this effect so that results could be compared to the 1D model.

Two particle system

To demonstrate how the understanding the drying behavior can be exploited to develop novel coatings, a two particle system was dried. A bimodal silica dispersion containing particles of 1 μm in diameter and 200 nm in diameter was prepared with an overall particle volume fraction of 0.2. The coating had an initial thickness of 400 μm and was dried at 5 μm/min. The final result was a coating with a top layer entirely composed of smaller particles and a bottom layer of small particles dispersed between large particles (Figure 16).

The coating microstructure formation can be deduced from the drying regime map. Under the given conditions, the smaller silica particles were estimated to be in the evaporation regime, and the larger particles were estimated to be in the sedimentation regime. Therefore, as drying occurred, the smaller particles accumulated at the free surface of the coating in a drying front, whereas the larger particles sedimented toward the base. Those small particles that were not trapped in the consolidation front were scattered randomly throughout the sedimenting particles. Finally, enough water was lost from the coating that all particles were immobilized. The smaller particles that were trapped in the bottom of the coating were not small enough to move between the fully consolidated larger particles. Otherwise, reorganization of the smaller particles could have continued after the larger particles had reached their final packing fraction, as observed elsewhere.[29] This type of coating could be a cost effective strategy to introduce a large particle filler into a film of expensive small particles without reducing the final quality of the product.

The application of the drying map to this example assumes that the sedimentation coefficient and compressibility factor are the same for a two particle system as for a one particle system. This assumption is not valid for particles that are very different in size. Therefore, more work is

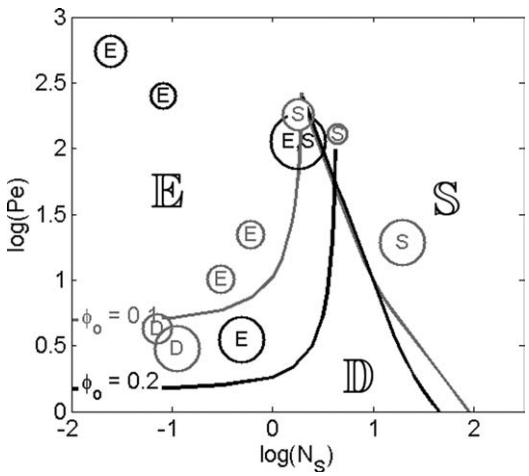

Figure 15. Drying map created from the theoretical model displaying points where evaporation (𝔼), sedimentation (𝕊), and diffusion (𝔻) regimes were discovered through CryoSEM for ϕ_0 = 0.1 (grey) and ϕ_0 = 0.2 (black).

Circle sizes denote the estimated magnitude of error.

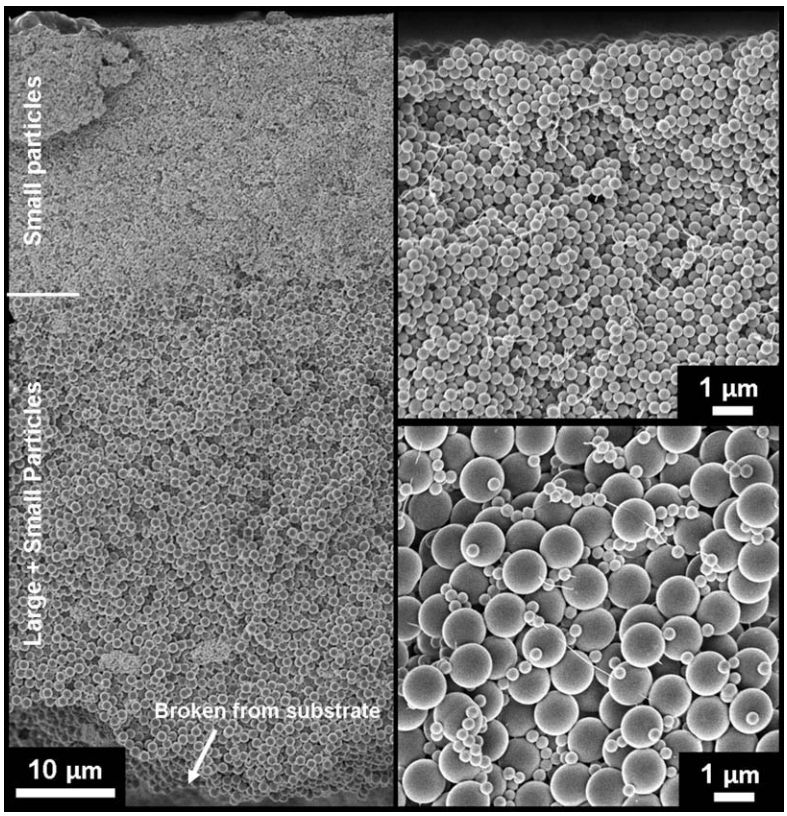

Figure 16. Cross-section image of a dried coating prepared from a bimodal aqueous silica dispersion.

Top right: higher magnification image of top of coating. Bottom right: bottom of coating.

required to rigorously adapt the drying map to more complicated systems.

Summary

The nonlinear 1D conservation equation with concentration dependent diffusion and sedimentation coefficients was solved for the concentration profiles at different time points for various drying conditions. This gave a picture of the particle distribution before air invades into the particle packing. From this data, a drying map, which related the observed behavior (sedimentation, diffusion or evaporation dominant) to two dimensionless numbers, Pe and N_s, was developed. It was then demonstrated that certain limiting cases of the drying map could be calculated analytically. CryoSEM was used as an experimental validation of the predicted drying behavior. This method produced visual verification of the predicted concentration profiles in the drying coating. Finally, it was demonstrated that by understanding its drying behavior a novel coating could be developed. It is hoped that this work will provide greater understanding of the drying process of particulate coatings and that it can be used to design drying conditions to produce desired coating microstructures.

Acknowledgments

The authors gratefully acknowledge funding from industrial sponsors of the Coating Process Fundamentals Program of the Industrial Partnership for Research in Interfacial and Materials Engineering at the University of Minnesota and also the BrainKorea21 Program (BK21) for support for Yoon Dong Jung. Parts of this work were carried out in the University of Minnesota I.T. Characterization Facility, which receives partial support from NSF through the NNIN program. Finally, the authors thank Prof. Satish Kumar for helpful discussions.

Literature Cited

1. Li G, Pickup PG. Ionic conductivity of PEMFC electrodes. *J Electrochem Soc*. 2003;150:C745–C752.
2. Ackerson BJ, Paulin SE, Johnson B, van Megen W, Underwood S. Crystallization by settling in suspensions of hard spheres. *Phys Rev E*. 1999;59:6903.
3. Wang W, Gu B, Liang L, Hamilton W. Fabrication of two- and three-dimensional silica nanocolloidal particle arrays. *J Phys Chem B*. 2003;107:3400–3404.
4. Snyder MA, Lee JA, Davis TM, Scriven LE, Tsapatsis M. Silica nanoparticle crystals and ordered coatings using lys-sil and a novel coating device. *Langmuir* 2007;23:9924–9928.
5. Chapman D. Coating structure effects on ink-jet print quality. In: TAPPI Coating Conference Proceedings. Atlanta: TAPPI press, 1997:73.
6. Ma Y, Davis HT, Scriven LE. Microstructure development in drying latex coatings. *Prog Org Coat*. 2005;52:46–62.
7. Routh AF, Russel WB. Horizontal drying fronts during solvent evaporation from latex films. *AICHE J*. 1998;44:2088–2098.
8. Routh AF, Zimmerman WB. Distribution of particles during solvent evaporation from films. *Chem Eng Sci*. 2004;59:2961–2968.
9. Sarkar A, Tirumkudulu MS. Consolidation of charged colloids during drying. *Langmuir* 2009;25:4945–4953.
10. Yiantsios SG, Higgins BG. Marangoni flows during drying of colloidal films. *Phys Fluids*. 2006;18:082103–082111.
11. Gorce JP, Bovey D, McDonald PJ, Palasz P, Taylor D, Keddie JL. Vertical water distribution during the drying of polymer films cast from aqueous emulsions. *Eur Phys J E: Soft Matter Biol Phys*. 2002; 8:421–429.

12. Ciampi E, Goerke U, Keddie JL, McDonald PJ. Lateral transport of water during drying of alkyd emulsions. *Langmuir* 2000;16:1057–1065.
13. Ekanayake P, Doughty P, Keddie JL, McDonald PJ. Experimental tests of scaling predictions of the spatial distribution of particles during the drying of colloidal films. *Magn Reson Imaging*. 2007; 25:557–557.
14. Schabel W, Ludwig I, Kind M. Measurements of concentration profiles in polymeric solvent coatings by means of an inverse convocal micro Raman spectrometer-Initial results. *Drying Technol*. 2004; 22:285–294.
15. Luo H, Cardinal CM, Scriven LE, Francis LF. Ceramic nanoparticle/monodisperse latex coatings. *Langmuir* 2008;24:5552–5561.
16. Kynch GJ. A theory of sedimentation. *Trans Faraday Soc*. 1952;48:166.
17. Buscall R, White LR. The consolidation of concentrated suspensions. *J Chem Soc Faraday Trans*. 1987;83:873–891.
18. Davis K, Russel W. An asymptotic description of transient settling and ultrafiltration of colloidal dispersions. *Phys. Fluids A*. 1989;1:82.
19. Davis RH, Birdsell KH. Hindered settling of semidilute monodisperse and polydisperse suspensions. *AICHE J*. 1988;34:123–129.
20. Russel WB, Davis KE. Settling suspensions of colloidal silica: observations and X-ray measurements. *J Chem Soc Faraday Trans*. 1991;87:411–424.
21. van Duijneveldt JS, Dhont JKG, Lekkerkerker HNW. Expansion and crystallization of a sediment of charged colloidal spheres. *J Chem Phys*. 1993;99:6941.
22. Russel WB, Saville DA, Schowalter WR. *Colloidal Dispersions*. Cambidge: Cambridge University Press, 1989.
23. Routh AF, Russel WB. Process model for latex film formation: limiting regimes for individual driving forces. *Langmuir* 1999;15:7762–7773.
24. Stöber W, Fink A, Bohn E. Controlled growth of monodisperse silica spheres in the micron size range. *J. Colloid Interface Sci*. 1968;26:62–69.
25. Bogush GH, Tracy MA, Zukowski CF IV. Preparation of monodisperse silica particles: control of size and mass fraction. *J. Non-Cryst Solids*. 1988;104:95–106.
26. Cairncross RA, Francis LF, Scriven LE. Predicting drying in coatings that react and gel: drying regime maps. *AICHE J*. 1996;42:55–67.
27. Gasperino D, Meng L, Norris DJ, Derby JJ. The role of fluid flow and convective steering during the assembly of colloidal crystals. *J Cryst Growth*. 2008;310:131–139.
28. Deegan RD, Bakajin O, Dupont TF, Huber G, Nagel SR, Witten TA. Capillary flow as the cause of ring stains from dried liquid drops. *Nature*. 1997;389:827–829.
29. Luo H, Scriven LE, Francis LF. Cryo-SEM studies of latex/ceramic nanoparticle coating microstructure development. *J. Colloid Interface Sci*. 2007;316:500–509.

Manuscript received July 21, 2009, revision received Nov. 3, 2009, and final revision received Jan. 20, 2010.